Suppression of Aluminum Dust Explosion by Ca(H$_2$PO$_4$)$_2$/RM Composite Powder with Core–Shell Structure: Effect and Mechanism

Junfeng Wang [1] (iD)**, Xiangbao Meng** [1,2,3,*] (iD)**, Ke Yan** [1] **and Jinshe Chen** [1]

[1]   College of Mining and Safety Engineering, Shandong University of Science and Technology, Qingdao 266590, China; jfwang@sdust.edu.cn (J.W.); yanke19970325@163.com (K.Y.); chenjins2010@163.com (J.C.)

[2]   Key Laboratory of Ministry of Education for Mine Disaster Prevention and Control, Shandong University of Science and Technology, Qingdao 266590, China

[3]   Yankuang Group, Jining 273500, China

*   Correspondence: mxb@sdust.edu.cn; Tel.: +86-1358-933-8024

check for updates

Abstract: A Ca(H$_2$PO$_4$)$_2$/RM composite powder suppressant with core–shell structure was prepared with modified red mud (RM) as the carrier and Ca(H$_2$PO$_4$)$_2$ as the loaded particles, using a solvent–antisolvent process, in an attempt to suppress aluminum dust explosion more effectively. The suppression effects of the Ca(H$_2$PO$_4$)$_2$/RM composite powder suppressant for aluminum dust flame propagation and for explosion overpressure were tested in a vertical glass tube test apparatus and a 20 L explosion vessel. The results show that the Ca(H$_2$PO$_4$)$_2$/RM composite powder suppressant was more effective in suppressing aluminum dust flame propagation and explosion overpressure than either Ca(H$_2$PO$_4$)$_2$ or RM powder alone. Finally, the suppression mechanism of the Ca(H$_2$PO$_4$)$_2$/RM composite powder suppressant was analyzed. On the one hand, a large amount of burning heat was absorbed through the decomposition of Ca(H$_2$PO$_4$)$_2$ and the melting phase transformation of the decomposition product; on the other hand, the strong isolation provided by the RM helped limit flame propagation. The strong adsorptivity of RM allowed this material to adsorb the radicals from the explosion reaction perfectly.

Keywords: Ca(H$_2$PO$_4$)$_2$/RM composite; aluminum dust explosion; suppressant; suppression mechanism

1. Introduction

Aluminum products are widely used in many industries across the globe. Aluminum dust resulting from the processing or fabrication of aluminum products can form suspended dust clouds in a closed or semi-closed production environment. Exposure of these dust clouds to ignition sources (e.g., electric sparks, open flames, or hot surfaces) with sufficient energy could lead to violent explosions [1–5]. The over 2000 °C maximum explosion temperature of aluminum dust, when coupled with explosion-induced overpressure, will cause considerable damages [6–8]. A recent example is the catastrophic aluminum dust explosion accident that hit Kunshan Zhongrong Metal Products Co., Ltd., Jiangsu Province, China, on 2 August 2014, which left 146 dead and 91 injured [9]. As such, mitigating or eliminating aluminum dust explosion is of great significance to guaranteeing the safe production for related aluminum product manufacturers.

Explosion suppression represents an effective means of preventing dust explosion; a high-performance suppressant can effectively mitigate or eliminate dust explosion. Nevertheless, unlike methane explosion or organic dust explosion, aluminum dust explosion is hard to suppress. Going et al. [10] noted that it has always been deemed as a tough job to suppress metal dust explosion.

Taveau et al. [11] observed that explosion of metal dust such as aluminum or magnesium dust is more difficult to suppress than that of organic dust, since they have higher flame temperature (T_f), maximum explosion pressure (P_{max}), explosibility index (K_{St}), and flame speed (S_f). Despite the many difficulties in suppressing aluminum dust explosion, however, many researchers have experimented on the suppression effects of a range of suppressants for aluminum dust explosion. Dastidar and Amyotte [12] compared the suppression effects of $NaHCO_3$ and $KHCO_3$ for aluminum dust explosion in a 1 m^3 and a 4.4 m^3 closed vessel and discovered that the two suppressants are equally effective. Jiang et al. [13,14] evaluated the suppression effects of ABC powder and $NaHCO_3$ for aluminum dust explosion in a 20 L spherical explosion test apparatus and an open-space dust explosion apparatus. They demonstrated that a lower concentration is needed for ABC powder to suppress aluminum dust explosion compared with $NaHCO_3$, but if ABC powder is inadequately prepared, the NH_3 produced out of ammonium dihydrogen phosphate decomposition can add to the explosion severity of aluminum dust instead. Jiang et al. [15] investigated the suppression effects of melamine cyanurate (MCA) and melamine polyphosphate (MPP) for the flame propagation of aluminum dust and revealed that melamine cyanurate (MCA) performs better in this respect. While these findings have contributed greatly to the exploration for high-efficiency aluminum dust explosion suppressants, few of them are related to composite powder suppressants due to the limitations in terms of method and purpose.

Selecting and developing high-efficiency aluminum dust explosion suppressants is highly necessary due to the strong destructive and hard-to-suppress nature of aluminum dust explosion. Explosion suppressants are generally classified as water mist suppressants and powder suppressants. Water mist suppressants are well able to suppress the explosion of most non-metal dusts, but they do not work well in suppressing aluminum dust explosion, since in a hot environment, water will react with aluminum dust and generate H_2, which will add to the explosion severity of aluminum dust. Comparatively, powder suppressants are more suitable for aluminum dust explosion. These suppressants are categorized as inert powders, chemically active powders, and composite powders. In the present study, a high-efficiency composite powder suppressant for suppressing aluminum dust explosion is developed. Selecting the carrier is the first step for developing a composite powder suppressant. Here, red mud (RM) is used as the carrying material. RM is defined as the pollutive waste discharged from alumina extraction in aluminum-making process. In general practice, an average of 1.0–2.0 t RM is yielded per ton of alumina produced. Composed of Fe_2O_3, Al_2O_3, SiO_2, and CaO, this material is characterized by dense micropores, large specific surface area, high temperature resistance, good heat absorptivity, and good levitation. It is very suitable for serving as the carrier for the purpose herein. $Ca(H_2PO_4)_2$ is an excellent suppressant of chemical activity of aluminum powder explosion. It can be combined with the RM carrier to form a novel composite powder suppressor.

At present, people have a clear understanding of the inhibitory effect and mechanism of some single inert powders and chemically active powders on aluminum powder explosion. However, the development and research of composite powder suppressant for suppressing aluminum powder explosion are still rare. In order to effectively suppress the explosion of aluminum powder, it is necessary to develop an excellent composite suppressant. In this study, in order to develop an excellent composite powder suppressant for suppressing aluminum powder explosion, $Ca(H_2PO_4)_2$/RM composite powder was prepared using inert powder RM as the carrier and chemically active powder $Ca(H_2PO_4)_2$ as the loaded particles. The suppression effects of the $Ca(H_2PO_4)_2$/RM composite powder for aluminum dust flame propagation and for explosion overpressure were investigated in a vertical glass tube test apparatus and a 20 L explosion vessel. The suppression mechanism of this composite powder was also analyzed.

2. Materials and Methods

2.1. Material Preparation

The micrometer aluminum dust used in our experiment was sourced from Nangong Terik Metal Products Co., Ltd., Hebei Province, China. The particle size distribution of the aluminum dust
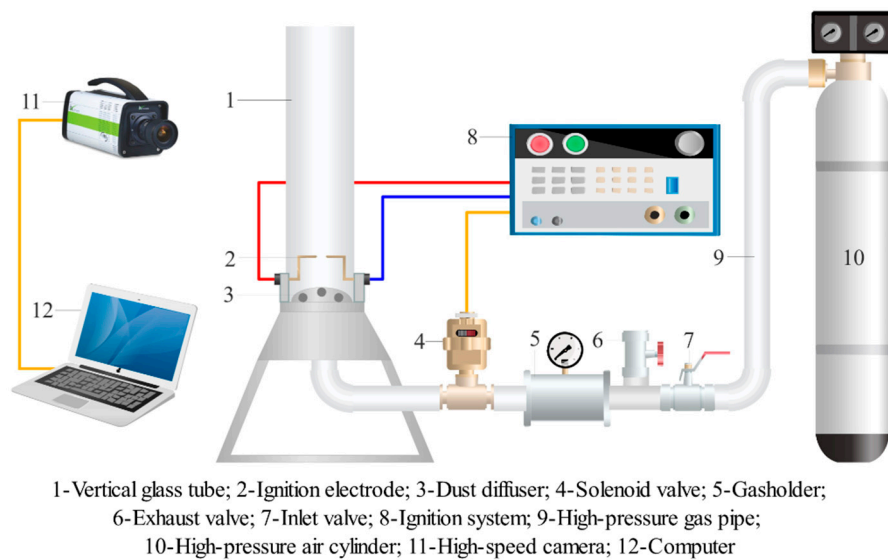
was measured using a Malvern Mastersizer2000 laser particle size analyzer (using wet method with water as a dispersant). The surface microstructure of the aluminum dust was also observed under a scanning electron microscope (SEM). Figure 1 shows the particle size distribution and SEM image of the aluminum dust. The RM used in our experiment was provided by Shandong Aluminum Industry Co., Ltd. Before the experiment, the RM was crushed and sieved to a particle size of less than 45 microns. The particles under the sieve were collected for further use. First, the RM was modified. Twenty-five grams of the sieved RM powder was dispersed into 100 mL distilled water. One hundred and fifty milliliters of 6 mol/L dilute hydrochloric acid were slowly added in and stirred for 2 h under a constant temperature of 85 °C. After the reaction solution had cooled down to room temperature, aqueous ammonia was dripped slowly in until the pH became 7.8 for the mixture to settle and gel. Then, 150 mL ethanol was added. The mixture was stirred for 0.5 h under a constant temperature of 50 °C and held still for 24 h so that the settlement was fully precipitated. During suction filtration, the mixture was rinsed repeatedly with distilled water to remove the unwanted ions in the settlement. After drying and grinding, the desired modified RM was yielded. Next, using the modified RM as the matrix, a $Ca(H_2PO_4)_2$/RM composite powder was prepared using solvent–antisolvent process. The preparation was completed in the following steps: (1) weigh 1.5 g of the $Ca(H_2PO_4)_2$ (analytically pure) to prepare saturated $Ca(H_2PO_4)_2$ solution; (2) weigh 5 g of the modified RM, disperse it into absolute alcohol and stir the solution magnetically to make it into a suspension; (3) under magnetic stirring, pour the prepared suspension into the saturated $Ca(H_2PO_4)_2$ solution; and (4) after adding all the suspension, continue to stir the mixture for 2 h, disperse it ultrasonically for 30 min, then age and settle it for 4 h. Filter out the settlement, vacuum dry it for 12 h under 30 °C, and finally yield the $Ca(H_2PO_4)_2$/RM composite powder suppressant.
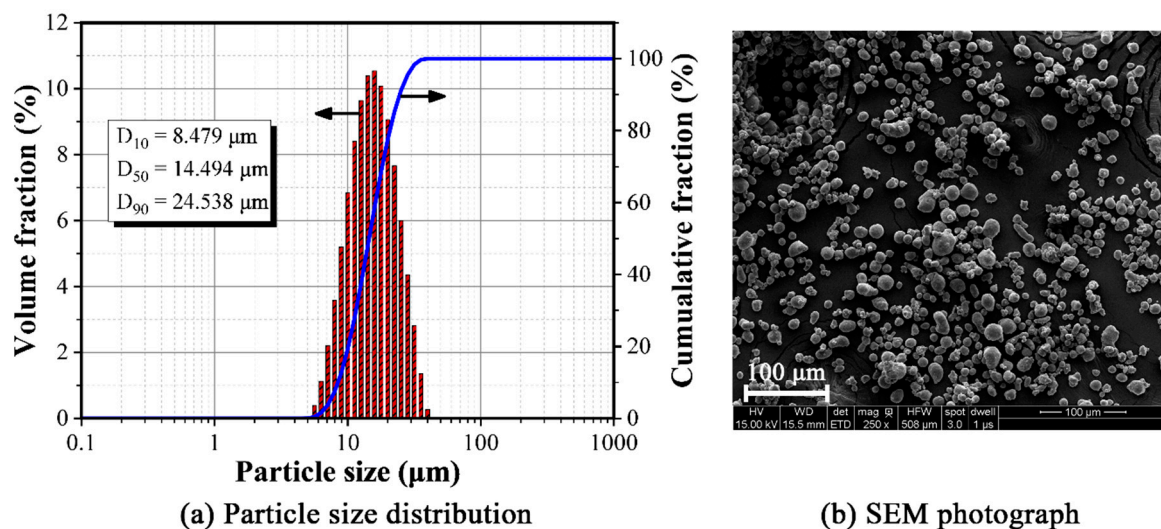
Figure 1. Particle size distribution and SEM photograph of aluminum dust: (**a**) Particle size distribution; (**b**) SEM photograph.

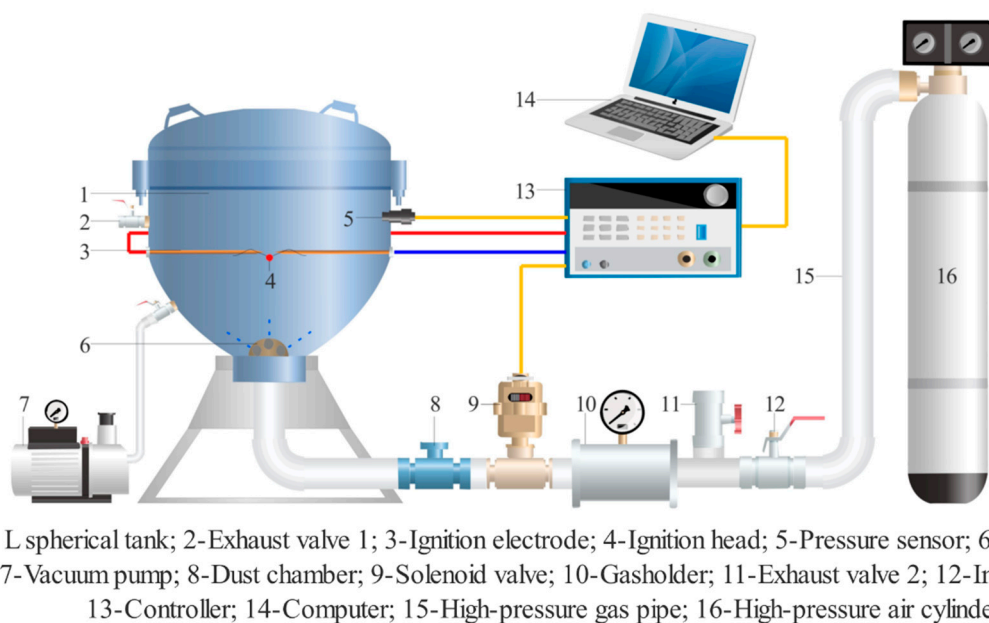*2.2. Flame Propagation Suppression Test*

An aluminum dust flame propagation test was conducted in a vertical glass tube test apparatus. As shown in Figure 2, this test apparatus was similar to that used in our previous study [16]. The quartz glass tube length was 600 mm and the diameter 68 mm. The dust injection pressure and ignition delay time were set to 0.3 MPa and 30 ms, respectively. During the experiment, 0.5 g of the aluminum dust and a given mass ratio of the suppressant were mixed up and uniformly spread on the umbrella-like dust diffuser. The ignition energy was set to 100 J. The START button was pressed to spray the dust sample into the vertical glass tube. After a 30 ms time, the ignition electrode produced 100 J electric sparks. The flame propagation was recorded by a high-speed video camera.

1-Vertical glass tube; 2-Ignition electrode; 3-Dust diffuser; 4-Solenoid valve; 5-Gasholder;
6-Exhaust valve; 7-Inlet valve; 8-Ignition system; 9-High-pressure gas pipe;
10-High-pressure air cylinder; 11-High-speed camera; 12-Computer

Figure 2. The vertical glass tube test apparatus.

2.3. Explosion Overpressure Suppression Test

The explosion overpressure suppression test was conducted in a 20 L explosion vessel. As shown in Figure 3, this test apparatus was the same as that used in our previous study [16]. The experiment was carried out according to the ASTM E1226 standard. Considering that overly high ignition strength may overdrive the 20 L explosion vessel, a pyrotechnic ignitor with a total mass of 0.48 g was used. This head can produce ignition energy of 2 kJ and maximum explosion pressure of 0.02 MPa. Before the experiment, 6 g of the aluminum dust and a given mass ratio of the suppressant were mixed up. During the experiment, we connected the pyrotechnic ignitor to the ignition lead and closed the explosion tank, and then we put the pre-weighted dust into the mixed dust chamber. The explosion vessel was vacuumed to −0.06 MPa, and the dust injection pressure was 2 MPa (gauge pressure). Then, the solenoid valve was activated by the computer, and the mixed dust was sprayed into the explosion tank. After a delay of 60 ms, the ignition head was ignited and, at the same time, the computer recorded the pressure data.

1-20 L spherical tank; 2-Exhaust valve 1; 3-Ignition electrode; 4-Ignition head; 5-Pressure sensor; 6-Dust diffuser;
7-Vacuum pump; 8-Dust chamber; 9-Solenoid valve; 10-Gasholder; 11-Exhaust valve 2; 12-Inlet valve;
13-Controller; 14-Computer; 15-High-pressure gas pipe; 16-High-pressure air cylinder

Figure 3. The 20 L spherical explosion test apparatus.

3. Results and Discussion

3.1. Structure and Characteristics of Composite Powder

The phase differences of the sample before and after compositing were compared under an X-ray diffractometer to compare the compositional changes in the powder material and examine the loading of $Ca(H_2PO_4)_2$. Figure 4 compares the X-ray diffraction (XRD) pattern between the RM and the composite powder loaded with $Ca(H_2PO_4)_2$. From these patterns, the characteristic XRD peak of the composite powder was essentially the same as that of the RM carrier; a characteristic XRD peak of the $Ca(H_2PO_4)_2$ crystals also appeared. The result indicated that the sample comprised a composite powder made up of $Ca(H_2PO_4)_2$ and RM.

The microstructure of the RM and the composite powder was observed under a SEM. Figure 5 shows the SEM photographs of the RM carrier and the composite powder. From these photographs, before loaded with the $Ca(H_2PO_4)_2$ particles, the surface of the RM particles were covered by the $Ca(H_2PO_4)_2$ crystals precipitated from recrystallization; the large amount of $Ca(H_2PO_4)_2$ crystals dispersed on the surface of the RM particles produced a microstructure similar to a core–shell structure. The SEM observation indicated successful compositing between $Ca(H_2PO_4)_2$ and RM through solvent–antisolvent process. The particle size distribution of the $Ca(H_2PO_4)_2$/RM composite powder was also measured with a Malvern Mastersizer2000 laser particle size analyzer (using wet method with ethanol as a dispersant). Figure 6 shows the particle size distribution of the $Ca(H_2PO_4)_2$/RM composite powder. The result indicates fairly uniform particle size distribution with a median particle size being around 4 μm.

The endothermic decomposition behavior of the RM and the composite powder was analyzed with a thermogravimetric analyzer (TGA). The experiment was performed under a range of temperatures from room temperature up to 800 °C, increased at the rate of 10 °C/min. Figure 7 shows the TG–DTG curves of the RM and the $Ca(H_2PO_4)_2$/RM composite powder samples. As can be observed, in the beginning, dehydration of the RM led to a quick weight loss in this material; later on, the TG curve of the RM began to fall steadily, with its total rate of weight loss being 18% at 800 °C. The $Ca(H_2PO_4)_2$/RM composite powder began to lose weight at 50 °C; the weight loss in the 50–120 °C interval is mainly attributable to the endothermic decomposition of the adsorbed water on the surface of the $Ca(H_2PO_4)_2$/RM composite powder; the weight loss in the 200–300 °C interval is attributable to the pyrolysis dehydration of the $Ca(H_2PO_4)_2$; the weight loss in the 600–700 °C interval relates to the dehydration of the iron, aluminum, and calcium hydroxides in the RM carrier into iron, aluminum, and calcium oxides; after the temperature reached 700 °C, the mass of the composite powder remained virtually unchanged, with the ultimate weight loss standing at around 23.2%.
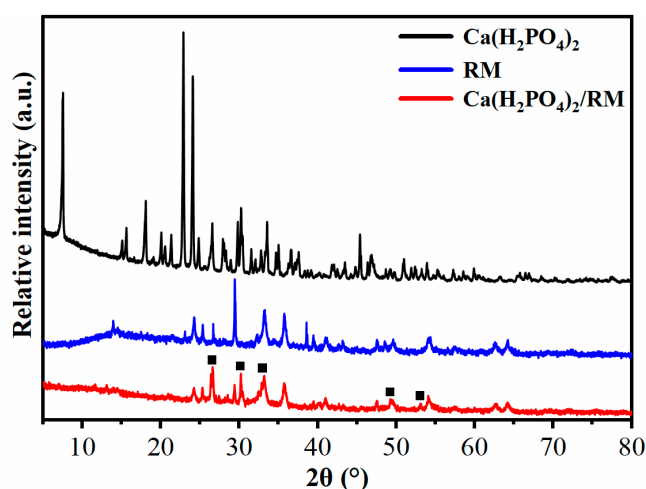

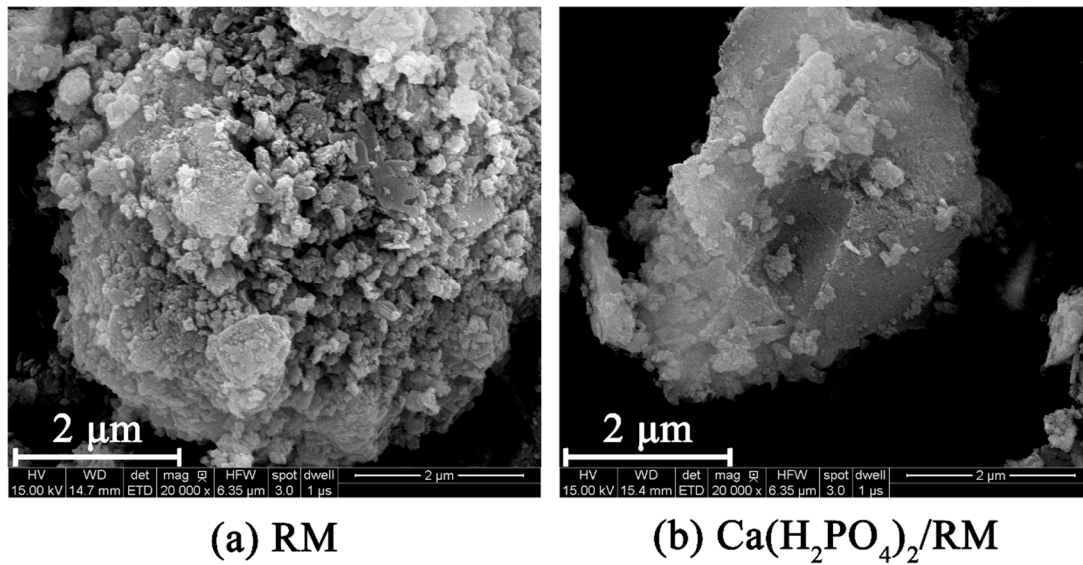**Figure 4.** XRD patterns of explosion suppressants.

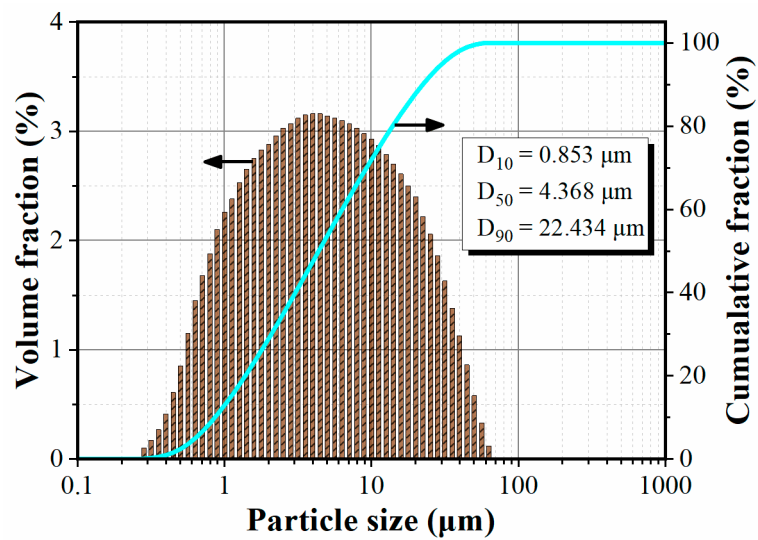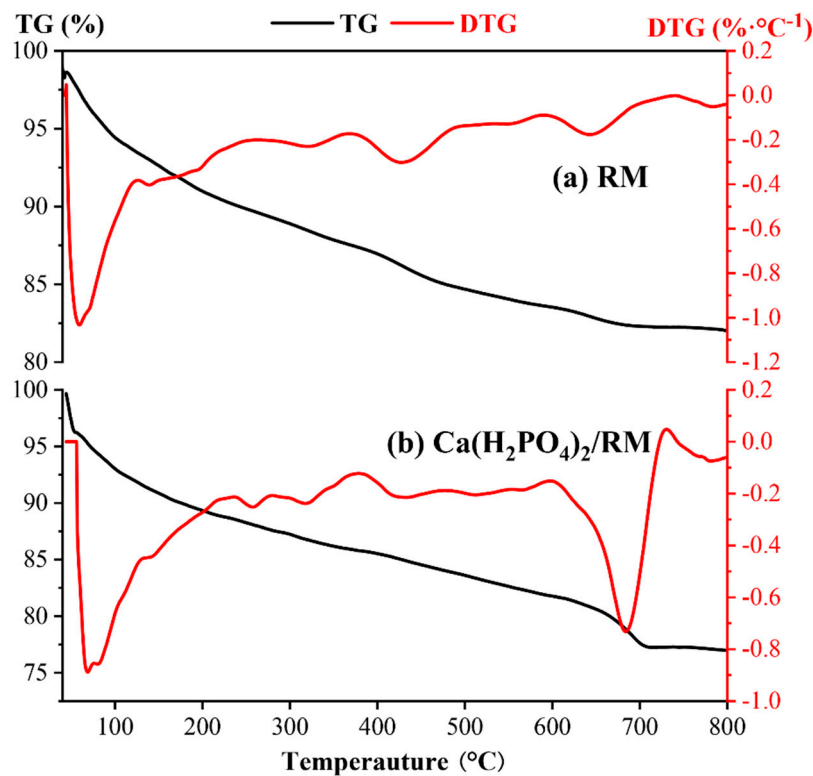**Figure 5.** SEM images of explosion suppressants.

Figure 6. Particle size distribution of $Ca(H_2PO_4)_2$/RM composite suppressant.

Figure 7. TG–DTG curves of red mud (RM) and Ca(H$_2$PO$_4$)$_2$/RM composite suppressants: (**a**) RM; (**b**) Ca(H$_2$PO$_4$)$_2$/RM.

3.2. Suppression Effect of Ca(H$_2$PO$_4$)$_2$/RM Composite Powder for Aluminum Dust Flame Propagation

Figure 8 shows the flame propagation process of the RM and the aluminum dust loaded with different proportions of suppressant after being ignited in a 600 mm long vertical glass tube. As shown in Figure 8a, the aluminum dust was highly explosive. After it was ignited, the aluminum dust cloud produced a blinding white light and the flame spread quickly, reaching the top of the glass tube at 50 ms. From Figure 8b, after the 20 wt% Ca(H$_2$PO$_4$)$_2$/RM composite suppressant was added, the flame propagation speed decreased remarkably and there was a 45 ms time delay for the flame to propagate up to the top of the glass tube. From Figure 8c, after 40 wt% Ca(H$_2$PO$_4$)$_2$/RM composite suppressant was added, the flame became obviously less bright, the flame propagation speed decreased remarkably and the maximum flame propagation distance was reduced. When 60 wt% Ca(H$_2$PO$_4$)$_2$/RM composite suppressant was added, the maximum flame propagation speed reduced remarkably (Figure 8d). From Figure 8e, after 80 wt% Ca(H$_2$PO$_4$)$_2$/RM composite suppressant was added, the aluminum dust flame propagation was essentially suppressed. From Figure 8e,e$_1$,e$_2$, the flame area of (e) was obviously smaller than that of (e$_1$) or (e$_2$), suggesting that the Ca(H$_2$PO$_4$)$_2$/RM composite suppressant was better able to suppress aluminum dust flame propagation than either Ca(H$_2$PO$_4$)$_2$ or RM powder alone. It is noted, however, that during the experiment, an obvious time lag was detected in the flame development after pure Ca(H$_2$PO$_4$)$_2$ was added and the initial flame intensity was quite weak (Figure 8e$_2$). This indicates that while Ca(H$_2$PO$_4$)$_2$ helped delay explosion development to some extent, it did not affect the ultimate flame length as much as the RM particles did. As shown in Figure 8e$_1$, adding 80 wt% RM worked well in suppressing the ultimate flame length. This is because the inert RM dispersed amid the aluminum dust particles helped block the heat transfer and contact among the aluminum dust particles, thereby limiting the flame propagation.
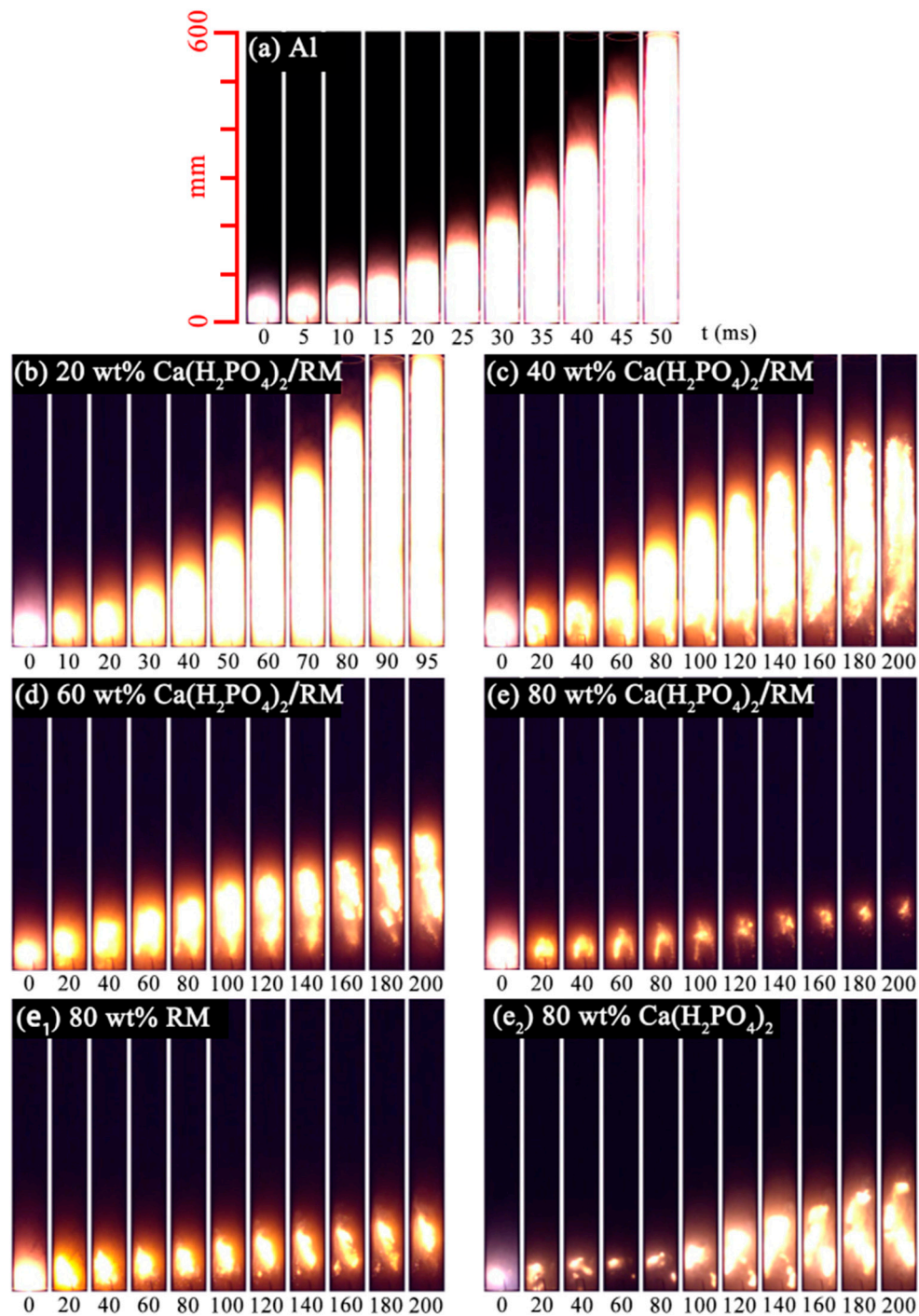
Figure 8. Suppression effect for aluminum dust explosion flame propagation among different suppressants.

3.3. Suppression Effect of for Aluminum Dust Explosion Overpressure

The typical explosion pressure histories obtained from the 20 L explosion vessel are shown in Figure 8. Two important characteristic parameters describing the dust explosion severity are marked: maximum explosion pressure (P_{max}) and maximum rate of explosion pressure rise ($(dP/dt)_{max}$) [16,17], which are major metrics for evaluating the suppression effect of an explosion suppressant. Burning time T_b is defined as the time between the ignition of the dust cloud and the maximum explosion pressure in the explosion tank [18]. Figure 9 shows the explosion criterion line. It is deemed that the suppressant had fully suppressed the explosion when the explosion overpressure was a maximum of 0.05 MPa(g) [19,20].

A series of explosion suppression tests was conducted in a 20 L explosion vessel. The explosion suppression performance of the $Ca(H_2PO_4)_2$/RM composite powder was tested at mass concentration 300 g/m^3 of the aluminum dust. The results are given in Figure 10. It can be observed in Figure 10a that, as the $Ca(H_2PO_4)_2$/RM composite suppressant increased, the T_b increased while the P_{max} reduced. This concurs with what has been observed in Figure 8. The P_{max} and $(dP/dt)_{max}$ variations are presented in Figure 10b. When 40 wt% $Ca(H_2PO_4)_2$/RM composite suppressant was added, the $(dP/dt)_{max}$ reduced swiftly from 98.6 MPa/s for pure aluminum dust to 42.8 MPa/s, at a rate of 56.6%, whereas the P_{max} reduced mildly from 0.72 MPa for pure aluminum dust to 0.61 MPa, at a mere rate of 15.2%. As the content of the composite suppressant increased, the $(dP/dt)_{max}$ began to drop at a lower rate. The P_{max} reduced remarkably when 120 wt% $Ca(H_2PO_4)_2$/RM composite suppressant was added, dropping from 0.49 MPa to 0.315 MPa. When 200 wt% $Ca(H_2PO_4)_2$/RM composite suppressant was added, the P_{max} dropped to 0.062 MPa, which was already below the explosion criterion line. In the $Ca(H_2PO_4)_2$/RM composite suppressant, rapid decomposition and melting phase transformation of the $Ca(H_2PO_4)_2$ powder allows the suppressant to absorb a large amount of burning heat and largely reduce the $(dP/dt)_{max}$. The ability of the inert RM to serve as an effective blocker at a given concentration affects the heat transfer between the aluminum particles and leads to incomplete reaction. To compare the explosion suppression performance, a suppression test was conducted on 200 wt% pure $Ca(H_2PO_4)_2$ and 200 wt% pure RM, respectively. As shown in Figure 10a, the pressure curves of both 200 wt% pure $Ca(H_2PO_4)_2$ and 200 wt% pure RM were higher than the explosion criterion line; their P_{max} and $(dP/dt)_{max}$ were both higher than when 200 wt% $Ca(H_2PO_4)_2$/RM composite suppressant was added. This suggests that the $Ca(H_2PO_4)_2$/RM composite suppressant was more effective in suppressing explosion than either $Ca(H_2PO_4)_2$ or RM alone. More importantly, 200 wt% pure $Ca(H_2PO_4)_2$ had a higher P_{max} than 200 wt% pure RM, but had a lower $(dP/dt)_{max}$. This was similar to the flame behavior in Figure 8. As shown in Figure 8e$_1$,e$_2$, when $Ca(H_2PO_4)_2$ was added, the flame developed slowly in the beginning; when RM was added, the flame area reduced obviously in the late stage. This suggests that $Ca(H_2PO_4)_2$ is more effective in suppressing $(dP/dt)_{max}$ and RM is more effective in suppressing P_{max}.
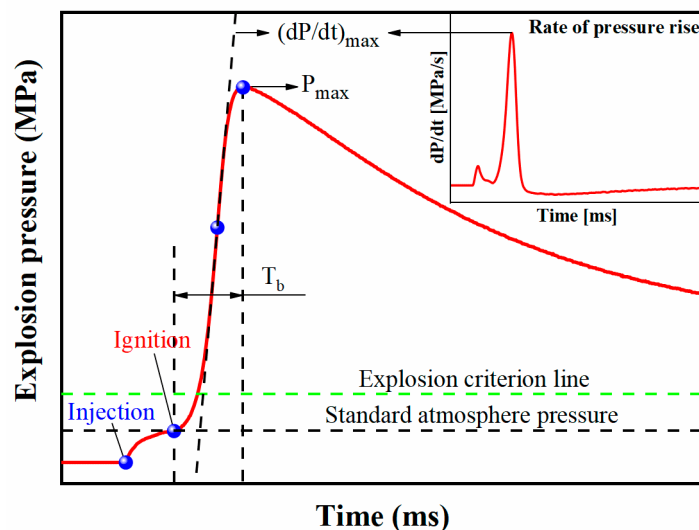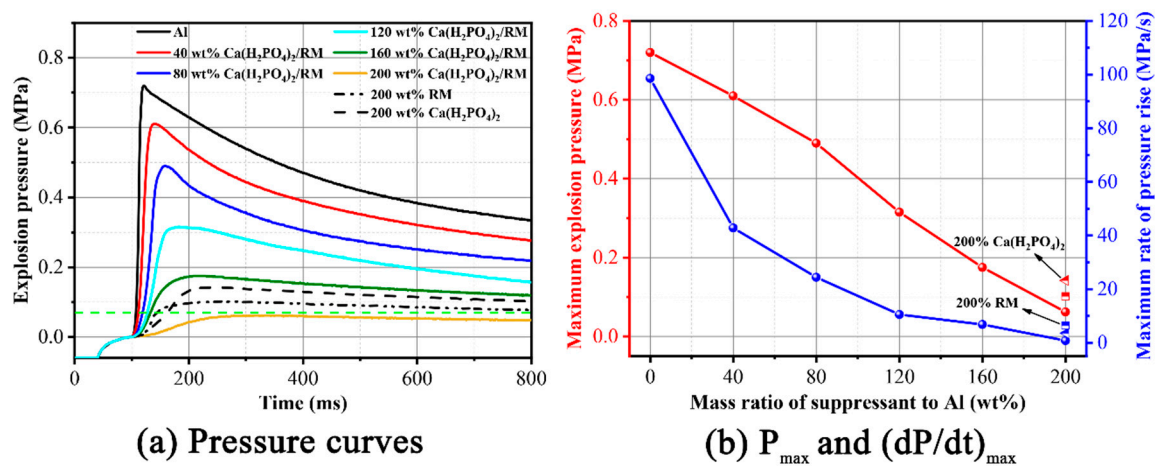

Figure 9. Typical explosion pressure time history.

Figure 10. Suppression effect between suppressants: (**a**) pressure curve and (**b**) P_{max} and $(dP/dt)_{max}$ values.

3.4. How Ca(H$_2$PO$_4$)$_2$/RM Composite Powder Suppresses Aluminum Dust Explosion

The microstructure of post dust-explosion products constitutes an important basis for examining the process and mechanism of dust explosion [21,22]. Figure 11 shows the photograph and SEM image of the aluminum dust explosion residue. From Figure 11a, the explosion residue comprises nanoscale spherical particles. In the light of previous studies, the process of aluminum dust explosion can be outlined as: after aluminum particles are heated, the Al$_2$O$_3$ film melts and ruptures, and non-uniform burning reaction occurs on the surface of the aluminum particles; as the temperature rises to 2700 K (boiling point for aluminum), aluminum vapor is generated, a violent gas phase burning reaction is triggered, and nanoscale Al$_2$O$_3$ particles are produced.

Figure 12 shows how the Ca(H$_2$PO$_4$)$_2$/RM composite powder suppresses aluminum dust explosion. The good dispersivity of the Ca(H$_2$PO$_4$)$_2$/RM composite powder, as well as its good ability to co-suppress explosion, helps improve the explosion suppression performance of the RM matrix and Ca(H$_2$PO$_4$)$_2$. The Ca(H$_2$PO$_4$)$_2$/RM composite powder was composed of two parts: Ca(H$_2$PO$_4$)$_2$ on the outside and the RM matrix at the core. During aluminum dust explosion, when the Ca(H$_2$PO$_4$)$_2$/RM composite powder encounters high temperature and explosive shock, the Ca(H$_2$PO$_4$)$_2$ particles coated on the surface of the RM matrix will begin to shed from the RM-base composite powder and suspend in the explosive space in full dispersion, whereas shedding of the surface particles will lead to more pore structures to expose in the RM matrix material itself. As explosion continues, the ambient explosion temperature will continue to rise. At that time, as the RM-base composite powder works to suppress the explosion reaction to a varying degree while continuing structural separation, in this hot environment, Ca(H$_2$PO$_4$)$_2$ will be decomposed into phosphate ions and calcium radicals; as temperature rises, the phosphate can break up into pyrophosphate and metaphosphoric acid, which will absorb a large amount of the reaction heat at each step of reaction, thereby reducing the ambient reaction temperature; phase transformation takes place in the resulted Ca$_2$P$_2$O$_7$ and CaPO$_3$ after further absorbing a large amount of heat. This helps dilute the aluminum and other radicals involved in the explosion reaction, thereby slowing down the explosion reaction. The exposed RM matrix dispersed across the space also serves as a good isolator and interrupter for flame propagation. Furthermore, the high porosity and strong adsorptivity of RM also allows the material to adsorb the radicals from the explosion reaction perfectly, which further suppresses the aluminum dust explosion.
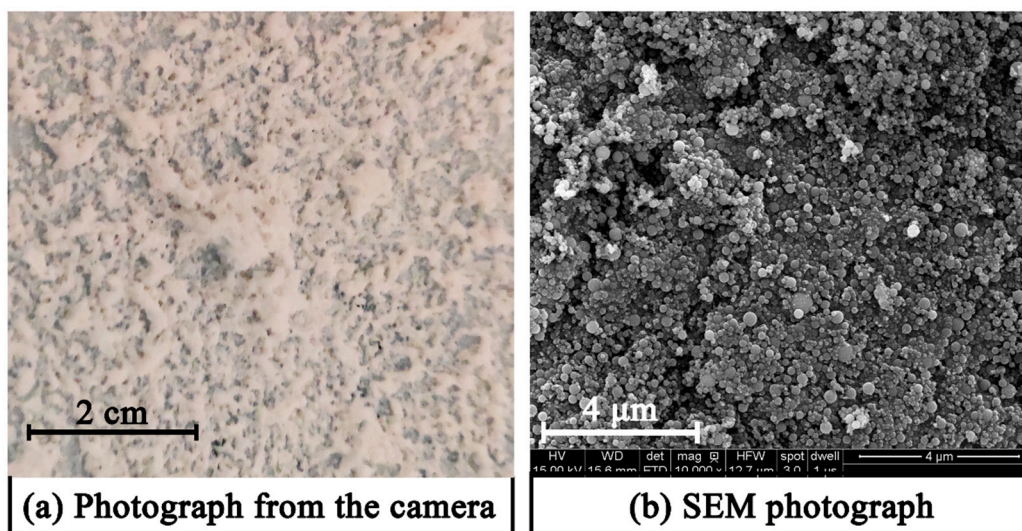
Figure 11. Photograph and SEM image of the aluminum dust explosion product.
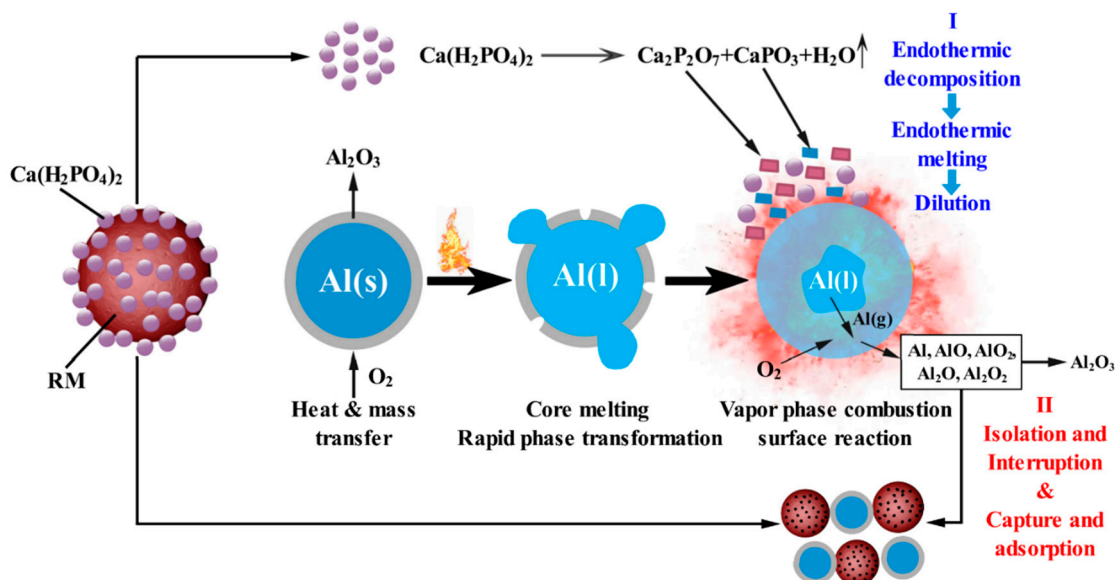

Figure 12. Sketch showing how $Ca(H_2PO_4)_2$/RM composite powder suppresses aluminum dust explosion.

4. Conclusions

A $Ca(H_2PO_4)_2$/RM composite powder was prepared from industrial waste RM as the carrier and $Ca(H_2PO_4)_2$ as the loaded particles, using a solvent–antisolvent process. The composite powder was tested by XRD and SEM. The result indicated that $Ca(H_2PO_4)_2$ particles were successfully loaded onto the surface of the RM particles and formed a unique core–shell structure of particles that were fairly uniform in size, with a median particle size being around 4 μm. Thermogravimetric analysis demonstrated good heat absorptivity for the $Ca(H_2PO_4)_2$/RM composite material.

An aluminum dust flame propagation test and an explosion suppression test were conducted in a vertical glass tube test apparatus and a 20 L explosion vessel; the explosion suppression performance of the $Ca(H_2PO_4)_2$/RM composite powder was also evaluated. The result showed that $Ca(H_2PO_4)_2$ was more effective in suppressing flame propagation speed and $(dP/dt)_{max}$, whereas RM was more effective in suppressing flame propagation distance and P_{max}. As the composite powder was well able to co-suppress explosion and had good dispersivity, the $Ca(H_2PO_4)_2$/RM composite powder suppressant performed better in suppressing an explosion than either $Ca(H_2PO_4)_2$ or RM alone.

The suppression mechanism of the $Ca(H_2PO_4)_2$/RM composite powder for aluminum dust explosion was analyzed. On the one hand, in a hot environment, $Ca(H_2PO_4)_2$ was endothermically decomposed into $Ca_2P_2O_7$ and $CaPO_3$. Further heat absorption of the resultant $Ca_2P_2O_7$ and $CaPO_3$ led to a phase transformation. This allowed the absorption of a large amount of heat from the aluminum dust explosion and helped dilute the radicals from the explosion reaction, thereby slowing down the explosion reaction. On the other hand, the porous RM dispersed across the space also served as a good isolator and interrupter that limited the flame propagation. Furthermore, as RM is porous and highly adsorptive, it can well adsorb the radicals from explosion reaction and further suppress aluminum dust explosion.

Author Contributions: Conceptualization, X.M. and J.W.; investigation, J.W. and K.Y.; data curation, J.C.; writing—original draft preparation, J.W. and K.Y.; writing—review and editing, X.M. and J.C.; project administration, X.M.

Conflicts of Interest: The authors declare no conflict of interest.

References

1. Marmo, L.; Piccinini, N.; Danzi, E. Small magnitude explosion of aluminium powder in an abatement plant: A telling case. *Process Saf. Environ.* **2015**, *98*, 221–230. [CrossRef]
2. Amyotte, P.R.; Eckhoff, R.K. Dust explosion causation, prevention and mitigation: An overview. *J. Chem. Health Saf.* **2010**, *17*, 15–28. [CrossRef]
3. Yuan, Z.; Khakzad, N.; Khan, F.; Amyotte, P. Dust explosions: A threat to the process industries. *Process Saf. Environ.* **2015**, *98*, 57–71. [CrossRef]
4. Li, Q.Z.; Wang, K.; Zheng, Y.N.; Mei, X.N.; Lin, B.Q. Explosion severity of micro-sized aluminum dust and its flame propagation properties in 20 L spherical vessel. *Powder Technol.* **2016**, *301*, 1299–1308. [CrossRef]
5. Li, Q.; Lin, B.; Li, W.; Zhai, C.; Zhu, C. Explosion characteristics of nano-aluminum powder–air mixtures in 20L spherical vessels. *Powder Technol.* **2011**, *212*, 303–309. [CrossRef]
6. Jiang, B.; Lin, B.; Shi, S.; Zhu, C.; Li, W. Explosive characteristics of nanometer and micrometer aluminum-powder. *Min. Sci. Technol.* **2011**, *21*, 661–666. [CrossRef]
7. Lin, B.Q.; Li, W.X.; Zhu, C.J.; Lu, H.L.; Lu, Z.G.; Li, Q.Z. Experimental investigation on explosion characteristics of nano-aluminum powder-air mixtures. *Combust. Explos. Shock Waves* **2010**, *46*, 678–682. [CrossRef]
8. Marmo, L.; Cavallero, D.; Debernardi, M.L. Aluminium dust explosion risk analysis in metal workings. *J. Loss Prev. Proc.* **2004**, *17*, 449–465. [CrossRef]
9. Li, G.; Yang, H.X.; Yuan, C.M.; Eckhoff, R.K. A catastrophic aluminium-alloy dust explosion in China. *J. Loss Prev. Proc.* **2016**, *39*, 121–130. [CrossRef]
10. Going, J.E.; Snoeys, J. Explosion protection with metal dust fuels. *Process Saf. Prog.* **2002**, *21*, 305–312. [CrossRef]
11. Taveau, J.; Vingerhoets, J.; Snoeys, J.; Going, J.; Farrell, T. Suppression of metal dust deflagrations. *J. Loss Prev. Proc.* **2015**, *36*, 244–251. [CrossRef]
12. Dastidar, A.; Amyotte, P. Determination of Minimum Inerting Concentrations for Combustible Dusts in a Laboratory-Scale Chamber. *Process Saf. Environ.* **2002**, *80*, 287–297. [CrossRef]
13. Jiang, H.; Bi, M.; Li, B.; Zhang, D.; Gao, W. Inhibition evaluation of ABC powder in aluminum dust explosion. *J. Hazard. Mater.* **2019**, *361*, 273–282. [CrossRef] [PubMed]
14. Jiang, H.P.; Bi, M.S.; Gao, W.; Gan, B.; Zhang, D.W.; Zhang, Q. Inhibition of aluminum dust explosion by NaHCO3 with different particle size distributions. *J. Hazard. Mater.* **2018**, *344*, 902–912. [CrossRef] [PubMed]
15. Jiang, H.; Bi, M.; Ma, D.; Li, B.; Cong, H.; Gao, W. Flame suppression mechanism of aluminum dust cloud by melamine cyanurate and melamine polyphosphate. *J. Hazard. Mater.* **2019**, *368*, 797–810. [CrossRef] [PubMed]
16. Wang, J.; Meng, X.; Ma, X.; Xiao, Q.; Liu, B.; Zhang, G. Experimental study on whether and how particle size affects the flame propagation and explosibility of oil shale dust. *Process Saf. Prog.* **2019**, *38*, e12075. [CrossRef]

17. Cao, W.G.; Qin, Q.F.; Cao, W.; Lan, Y.H.; Chen, T.; Xu, S.; Cao, X. Experimental and numerical studies on the explosion severities of coal dust/air mixtures in a 20-L spherical vessel. *Powder Technol.* **2017**, *310*, 17–23. [CrossRef]

18. Li, Q.Z.; Yuan, C.C.; Tao, Q.L.; Zheng, Y.N.; Zhao, Y. Experimental analysis on post-explosion residues for evaluating coal dust explosion severity and flame propagation behaviors. *Fuel* **2018**, *215*, 417–428. [CrossRef]

19. Yu, L.F.; Li, G.; Liu, W.C.; Yu, J.N.; Yuan, C.M. Experimental investigations on ignition sensitivity of hybrid mixtures of oil shale dust and syngas. *Fuel* **2017**, *210*, 1–7. [CrossRef]

20. Li, G.; Yuan, C.M.; Fu, Y.; Zhong, Y.P.; Chen, B.Z. Inerting of magnesium dust cloud with Ar, N2 and CO2. *J. Hazard. Mater.* **2009**, *170*, 180–183. [CrossRef]

21. Sen, H.S.; Liu, Z.T.; Zhao, E.L.; Lin, S.; Qiu, L.M.; Qian, J.F.; Liu, H.X.; Xia, S.K. Comparison of behavior and microscopic characteristics of first and secondary explosions of coal dust. *J. Loss Prev. Proc.* **2017**, *49*, 382–394. [CrossRef]

22. Liu, Z.T.; Lin, S.; Zhang, S.S.; Wang, E.Y.; Liu, G.H. Observations of microscopic characteristics of post-explosion coal dust samples. *J. Loss Prev. Proc.* **2016**, *43*, 378–384. [CrossRef]